The Investigation of Hollow Gold Nanoparticles as a Targeted Drug Delivery System

Antonio Rios

Senior Comprehensive Project

April 11, 2025



Allegheny College, Department of Biochemistry

Submitted to the Department of Biochemistry of Allegheny College in partial fulfillment of the requirement for the degree of Bachelor of Science.

The Investigation of Hollow Gold Nanoparticles as a Targeted Drug Delivery System

Antonio Rios

Senior Comprehensive Project

Allegheny College Class of 2025

Committee Members:

Dr. Alice Deckert

Dr. Margaret Nelson

Dr. Elizabeth Guldan

I hereby recognize and pledge to fulfill my responsibilities, as defined in the Honor Code, and to maintain the integrity of both myself and the College community as a whole.

Pledge: 

The Investigation of Hollow Gold Nanoparticles as a Targeted Drug Delivery System

Table of Contents

ACKNOWLEDGEMENTS……4

ABSTRACT……5

INTRODUCTION……...6

Figure 1……..11

Figure 2……..13

Figure 3 ……14

Figure 4……..15

EXPERIMENTAL……20

RESULTS AND DISCUSSION……23

Figure 5……..24

Figure 6……..25

Table 1……...26

Figure 7……..26

Figure 8……..27

Table 2……...27

FUTURE DIRECTIONS……...30

CONCLUSION……..31

RESOURCES……32

Acknowledgements

I would like to first thank Dr. Deckert for her invaluable guidance, encouragement, and support throughout this project. Her insight and patience were instrumental in not only guiding me throughout the research but also shaping my growth as both a student and a scientist. I am also grateful to Dr. Nelson and Dr. Guldan for serving as my readers and for taking the time to provide thoughtful feedback and support.

I want to thank my Papa, Mama, sisters, Isa and Sofia, and Grandpa for being my unwavering support system through every step of my journey at Allegheny College. Your belief in me gave me the strength to persevere through every challenge, and I will continue striving to make you proud as I begin the next chapter of my education at LECOM. A special shoutout to my dog Monty, for being my favorite Rios sibling.

Finally, I'd like to thank the Allegheny College baseball team for being my second family, and a constant source of motivation. This experience would not have been the same without you, and I will forever cherish the memories I've made as a Gator baseball player. I wouldn't trade the 6am lifts, mile runs, tarp pulls, Gator Grit challenges, or late nights for anything. I am forever grateful to Coach Crum, Coach Rowe, Coach Claus, Coach Schuch, and Coach Jones, for making these the most enjoyable four years of college. Shoutout to Brady, Alex, Matt, Tyson, Walker, and Ty—brothers for life.

Abstract

Silver nanoparticles were synthesized using sodium borohydride and employed in a galvanic replacement reaction to produce hollow gold nanoparticles. The resulting hollow gold nanoparticles exhibited a resonance peak at 976nm, consistent with their hollow morphology and localized surface plasmon resonance properties. These characteristics make them promising candidates for drug delivery systems and targeted cancer therapies. To simulate drug loading, Methyl Orange and Acid Orange 5 were used as dye analogs for small-molecule drugs. This study confirms the feasibility of dye loading into Tween 20-stabilized hollow gold nanoparticles. Langmuir Isotherm modeling was used to evaluate loading behavior, yielding a maximum loading capacity of 62.19 and an equilibrium constant of 0.016 for Acid Orange 5, while Methyl Orange exhibited a maximum loading capacity of 56.67 and an equilibrium constant of 0.019. The Langmuir model fit well for Acid Orange 5 but not for Methyl Orange, which was linear at low concentrations, suggesting behavior more indicative of a very high K value and a system approaching saturation rapidly. These results demonstrate how dye structure and surface functionalization influence loading efficiency and binding behavior, offering insight into the optimization of nanoparticle-based drug delivery systems.

Introduction

In their lifetime both men and women in the United States have about a 40 percent chance of developing invasive cancer.[1] There are more than 200 types of cancer, most of which do not have a cure.[2] One major feature of cancer is the rapid growth and spread of abnormal cells to healthy organs and tissues, taking up nutrients and space that healthy organs need to function.[2] This process is called metastasis and is the primary cause of death from cancer.[2] Many forms of treatment are being studied including chemotherapy, radiation therapy, surgical intervention, and targeted therapy.[3] Most patients receive a combination of treatments.[4]

Chemotherapy is a common cancer treatment that uses powerful drugs to kill or inhibit the growth of cancer cells by targeting fast-dividing cells.[3,4] The primary advantage of chemotherapy is the ability to target fast-dividing cells, making it effective for many types of cancer.[3,4] It can potentially shrink tumors, alleviate symptoms, and increase survival rates. However, chemotherapy also has significant downsides.[3–5] It often causes severe side effects, including fatigue, nausea, hair loss, and a weakened immune system, which can impact the patient's quality of life.[3,4] Additionally, chemotherapy may not be effective for all cancers, and there's a risk of resistance developing.[3,4]

Therapies involving radiation are a widely used treatment for cancer that use high-energy particles or waves to destroy or damage cancer cells.[3] A significant advantage is the ability to target specific areas of the body which minimizes damage to surrounding healthy tissue.[3] This precision can lead to effective tumor shrinkage and symptom relief, and it is often used in combination with surgery or chemotherapy to enhance treatment outcomes.[3] However, radiation therapy also has drawbacks.[3] Patients may experience side effects such as fatigue, skin irritation, and, in some cases, long-term changes in the treated area, such as fibrosis or secondary cancers.[3]

Additionally, radiation is not suitable for all types of cancer, particularly those that are not localized.[3]

Surgical intervention is another primary treatment for many cancers, as it offers the potential for the complete removal of tumors and affected tissues.[3] One of its main advantages is the immediate physical removal of cancer, which can lead to significant improvement in survival rates, especially if the cancer is detected early.[3] Surgery can also provide relief from symptoms caused by tumors pressing on other organs.[3] However, there are notable downsides to consider. Not all cancers are operable due to their location or stage.[3] Even successful surgeries can require further treatments like chemotherapy or radiation to address any remaining cancer cells.[3] Surgery itself also carries risks of complications, such as infection and bleeding.[3]

Targeted therapy is a type of cancer treatment that uses drugs to precisely identify and attack cancer cells.[3,6,7] This approach targets specific molecules such as proteins, genes, or the tissue environment that contributes to the growth and survival of cancer cells.[3,6,7] Targeted therapy is better compared to other approaches because of the precision of the treatment which leads to greater effectiveness and fewer side effects.[6,7] It can also be personalized, as treatment can be tailored based on the specific genetic makeup of a patient's tumor.[5–7]

Nanotechnology has become an essential tool in delivering these drugs precisely to the cancer cells and is also used in the processes of disease diagnosis and therapy[8]. The unique properties of nanoparticles (NP) enable the precise delivery of therapeutic agents directly to cancer cells.[8] This precision comes from the ability of nanoparticles to be engineered at the nanoscale, which allows them to interact effectively with biological systems.[8] Studies indicate that the size of these nanoparticles facilitates their uptake into cells through endocytosis and enables direct translocation to reach intracellular and subcellular targets.[9,10] One type of

nanoparticle that has gained interest for cancer therapy is hollow gold nanoparticles (HAuNPs), which is a desirable form of nanoparticles due to their surface-to-volume ratio and high permeability.[11–13] Their hollow structure makes them well-suited for drug loading, enabling the encapsulation and controlled release of chemotherapeutic agents at the intended location inside of the patient's body.[11–14] If the drug is bound to the outside of the nanoparticle there is a greater chance of disassociation in the body before the nanoparticle reaches its target, causing the treatment to be less successful.[11,13] Once the nanoparticle reaches its intended location, the drug payload is released upon interacting with the cancer cells.[11,13]

Antibodies or other targeting molecules, such as peptides, can be grafted onto the surface of hollow nanoparticles to guide them specifically to cancer cells.[11] These targeting molecules are designed to recognize and bind to particular receptors overexpressed on the surface of cancer cells, which are often absent or present in lower amounts on normal cells.[11] When the nanoparticles are introduced into the body, the targeting molecules on their surface seek out and bind to these receptors.[11] This binding directs the nanoparticles to accumulate at the tumor site, enhancing the precision of drug delivery.[11] This targeted delivery system is crucial for the success of nanoparticle-based cancer therapies, as it enables the drug payload within the nanoparticles to be delivered directly to cancer cells.[11]

The penetration of IR light allows the payload inside of the nanoparticle to be released.[14] When near-infrared (NIR) light is directed at nanoparticles, especially those made of materials like gold, these nanoparticles absorb the light energy and convert it into heat through a process called photothermal conversion.[14] Gold nanoparticles can rapidly increase in temperature when exposed to NIR light.[14] NIR light can penetrate biological tissues more effectively than visible light because of its longer wavelength which helps it scatter less as it passes through tissues.[14]

This makes NIR light ideal for reaching deeper tissues without causing significant damage to the surrounding cells.[14] *Dung et al.* determined that NIR light between 650–900nm is preferred for photo-thermal cancer therapy because both blood and soft tissues are highly transparent within this range.[15]

Hollow nanoparticles represent a promising advancement in cancer therapy, yet the specific characteristics that a drug molecule needs for efficient loading into a nanoparticle are not well understood.

Hollow gold nanoparticles loaded with Doxorubicin, a chemotherapy drug, have demonstrated significant potential for targeted cancer therapy, particularly when combined with NIR light-triggered drug release.[16–18] A study by *You et al.* showcases the use of HAuNPs, approximately 40nm in diameter, that achieve an exceptionally high Doxorubicin payload of up to 63% by weight.[16] This was accomplished by leveraging the large surface area of the hollow structure, allowing Doxorubicin to attach to both the inner and outer surfaces of the HAuNPs.[16] Upon NIR laser irradiation, the HAuNPs generate heat, which rapidly releases Doxorubicin in a controlled manner.[16] This release is enhanced in acidic environments, such as the tumor microenvironment, making the system highly specific to cancerous tissues.[16] In vitro studies showed that NIR irradiation of Doxorubicin-loaded HAuNPs led to significant cancer cell killing.[16] A second study by *Sheth et al.* showed that unlike Doxorubicin loaded into HAuNPs, Doxorubicin-coated solid gold NPs do not respond to NIR laser irradiation to release the drug.[17] These results suggest that plasmon absorption of the NIR light and subsequent elevation of temperature around Doxorubicin-loaded HAuNPs mediates the release of Doxorubicin.[16,17]

Other drugs like Paclitaxel and Cisplatin have been successfully used for nanoparticle-targeted therapy.[19,20] Paclitaxel was loaded into HAuNPs through a double-emulsion solvent

evaporation technique, where Paclitaxel was trapped inside polymeric microspheres which serve as the primary drug carrier, encapsulating Paclitaxel within their matrix.[19] In this system, HAuNPs are embedded within the polymeric microspheres, acting as a photothermal agent that triggers drug release when exposed to NIR light.[19] Alternatively, Cisplatin was directly absorbed into the hollow cavity of the HAuNPs.[20] The drug was loaded through electrostatic interactions where the positive charges on Cisplatin are attracted to the negatively charged gold nanoparticle surface.[20] This attraction facilitates the initial adsorption of Cisplatin molecules onto the HAuNPs.[20] Additionally, coordination bonding between the amine groups in Cisplatin and the gold surface forms a metal-ligand coordination bond, which is stronger than electrostatic interactions.[20] Although these drugs have all shown success in loading a drug molecule into a HAuNP, no clear generalizations can be made because the conditions and nanoparticle characteristics differ in all four of the studies.

This study aims to further examine the loading efficiency of a series of dye molecules acting as a drug model with different bulk and polarity while keeping the nanoparticle characteristics and loading conditions constant throughout dye loading to determine if hollow gold nanoparticles have a loading capacity. This study will determine if there is a limit on the amount of a drug molecule that can be loaded in (or on) the nanoparticle for targeted therapy treatments by determining the maximum loading capacity of a HAuNP. By testing multiple trials with progressively higher concentrations of dye, the loading curve of the HAuNP can be accurately mapped out, which represents how much dye it can hold at different concentrations. The goal of this study is to identify the factors that increase the equilibrium constant, which reflects a high binding affinity between the dye and the nanoparticle. A larger equilibrium constant implies that the HAuNP reaches its maximum dye loading with lower dye

concentrations. Understanding this will help us optimize HAuNPs for targeted drug delivery applications, and we can better understand the physical and chemical properties that influence drug encapsulation and release. This knowledge is needed to develop nanoparticles that release drugs at a controlled rate once they reach their target, maximizing therapeutic effects while minimizing damage to healthy cells.

The synthesis of HAuNPs is most commonly done using galvanic replacement reactions, a type of redox reaction, in which a more reactive metal is replaced by a less reactive metal in a solution.[21] Galvanic replacement is driven by the difference in electrochemical potential between a solid metal, which has a lower reduction potential, and another metal ion, which has a higher reduction potential.[21] HAuNPs are most commonly synthesized using AgNPs, as shown in Figure 1.[21] This involves a two-step process where first, AgNPs are synthesized, and then, gold is added to the solution in the form of chloroauric acid ($HAuCl_4$).[21]

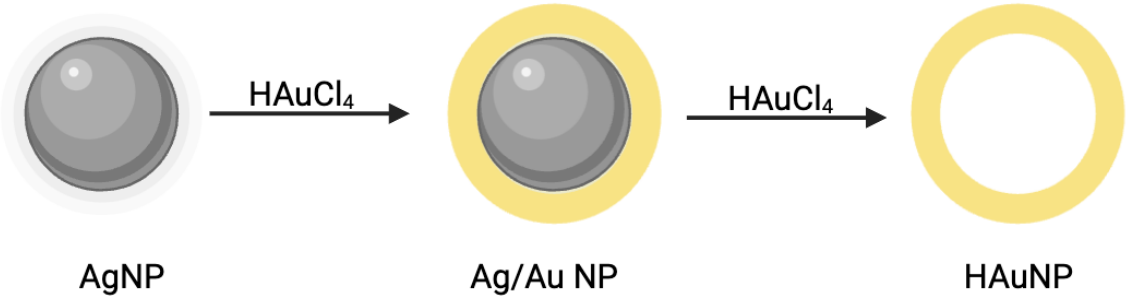


Figure 1. A schematic illustration of the synthesis of HAuNPs using AgNPs. The addition of $HAuCl_4$ will oxidize AgNPs to a silver-core gold-shell NP. Further addition of $HAuCl_4$ will oxidize the remaining silver, leaving HAuNPs.

The synthesis of AgNPs was done using a reducing agent and the strength of the reducing agent affects the synthesis of the NPs.[22] Sodium borohydride ($NaBH_4$) is a strong reducing agent

commonly used for this purpose.[22] This synthesis utilizes a reduction reaction in which silver nitrate ($AgNO_3$) serves as a source of silver ions (Ag^+) that get reduced to silver atoms (Ag^0) by $NaBH_4$.[22] $NaBH_4$ donates electrons to the silver ions, leading to the formation of silver nanoparticles (Equation a).[22]

$$2AgNO_{3\ (aq)} + 2NaBH_{4\ (aq)} \rightarrow 2Ag^{0}_{(s)} + 2NaNO_{3\ (aq)} + B_2H_{6\ (g)} + H_{2\ (g)} \quad \text{(a)}$$

The reduction process with $NaBH_4$ impacts the shape, size, and stability of the AgNPs.[23] However, because $NaBH_4$ is used in excess during the synthesis, it must be quenched and removed to prevent further reduction, as the excess $NaBH_4$ could reduce other metal ions, such as gold, in the case of mixed-metal NP formation.[23] If $NaBH_4$ is not properly quenched, it could result in a solution containing both silver and gold nanoparticles, rather than just gold replacing silver to form pure gold NPs.[23] Quenching is achieved by washing the nanoparticles by centrifuging and removing the supernatant containing excess $NaBH_4$, followed by replacing the supernatant with ultrapure water.[23] This process can be repeated multiple times to ensure thorough removal of residual $NaBH_4$ and any byproducts, leaving the nanoparticles stabilized in a clean solution.[23]

In nanoparticle synthesis, a capping agent is essential to stabilize the particles in solution.[24] Tween 20 makes for a great capping agent and plays a vital role in ensuring the stability of the NPs.[24,25] Capping agents, like Tween 20, are amphiphilic molecules with a hydrophilic (polar) head and a hydrophobic (nonpolar) tail (Figure 2).[24] The hydrophobic tail interacts with the surface of the nanoparticle, while the hydrophilic head faces the surrounding aqueous medium.[24] Since the NPs are in a polar water solution, Tween 20's nonpolar tail binds to the surface of the NPs, while the polar head interacts with the solvent.[24]

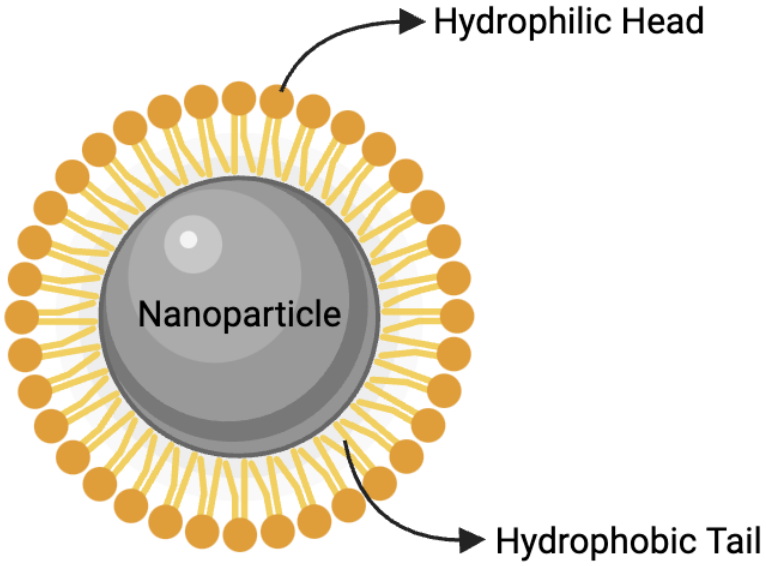


Figure 2. A capping agent bound to a nanoparticle via hydrophobic interactions.

Capping agents like Tween 20 provide several benefits. They stabilize nanoparticles in solution by preventing aggregation and ensuring a more uniform distribution.[24,25] This is crucial because, without a capping agent, the Van der Waals forces between the particles could cause them to aggregate and form large clusters.[24] By surrounding the particles with a capping agent, repulsive interactions, either electrostatic or steric, prevent the particles from coming into close contact, thus reducing aggregation.[24] This stabilization enhances the potential for the nanoparticles to be used in applications such as targeted drug delivery.[24]

Tween 20 (Figure 3) was chosen as the capping agent in this study because it effectively stabilizes the nanoparticles without the toxic effects associated with other agents.[24] Since Tween 20 is a Lewis base, it can interact with the surface of the AgNPs, binding to the particles while being soluble in the aqueous environment.[24]

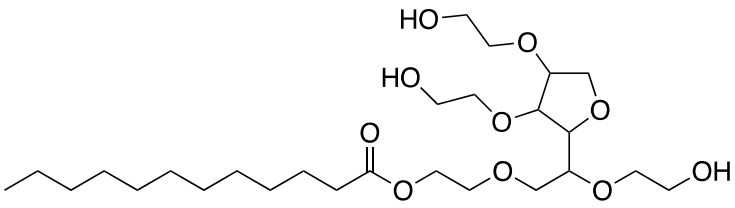


Figure 3. Structure of Tween 20.

$HAuCl_4$ is the primary source of gold ions (Au^{3+}) in the reaction, supplying these ions to participate in the redox process.[21] When $HAuCl_4$ is introduced to the AgNP solution, the metal with the lower potential (silver) is oxidized and transformed into a metal ion, from Ag to Ag+, and the metal ion with the higher potential (gold) is reduced and transformed into a solid metal, from Au^{3+} to Au, at the contact surface.[22] Through these processes, HAuNPs can be successfully synthesized.[21,22] The reduction of gold ions is facilitated by the higher reduction potential of $HAuCl_4$ compared to the silver oxidation potential, making the reaction thermodynamically favorable.[22] The oxidation state of the gold influences this reaction so that for every 1 gold atom, 3 silver ions are displaced from the nanoparticle until a solid shell of gold is formed. [22]

$$3Ag_{(s)} + AuCl_4^-{}_{(aq)} \rightarrow Au_{(s)} + 3Ag^+{}_{(aq)} + 4Cl^-{}_{(aq)} \quad \text{(b)}$$

Through the galvanic replacement reaction (Equation b), the gold progressively replaces the silver in the nanoparticle core.[21] This replacement continues until the silver core is dissolved and removed, leaving behind a hollow gold nanoshell.[21]

Drug loading into hollow NPs involves combining the drug molecules with the NP in solution, followed by processes such as sonication, heating, or stirring to encourage the drug molecules to enter the inner cavity.[26] Sonication was chosen for its simplicity, speed, and effectiveness in promoting nanoparticle–solute interactions without significantly altering particle structure. Previous studies have shown that while sonication, heating, and stirring can all enhance drug loading, the differences in loading efficiency among these methods are often

negligible under similar conditions.[27] Therefore, sonication was selected based on both its operational efficiency and widespread use in comparable nanoparticle loading protocols. Dyes are used as a replacement for drug molecules for the ease of measuring the loading capacity of HAuNPs.[26] A measured concentration of dye is added to the HAuNPs in solution, and the UV-Vis spectrum is measured using a UV-Vis spectrometer. Comparing the concentration of dye added to the solution, to the concentration of dye in the solution after encapsulation, the loading capacity of dye on/in the HAuNPs can be measured. Dye no longer in solution is either in the cavity of the HAuNP or bound to the surface of the particle.

Methyl Orange and Acid Orange 5 were chosen based on their structure, polarity, bulk, and weight, which closely mimic key characteristics of drug molecules. Both dye's molecular weights are around 300g/mol, Methyl Orange at 327.34g/mol, and Acid Orange 5 at 375.4g/mol, which is important because the majority of drug molecules fall below 500g/mol.[28,29]

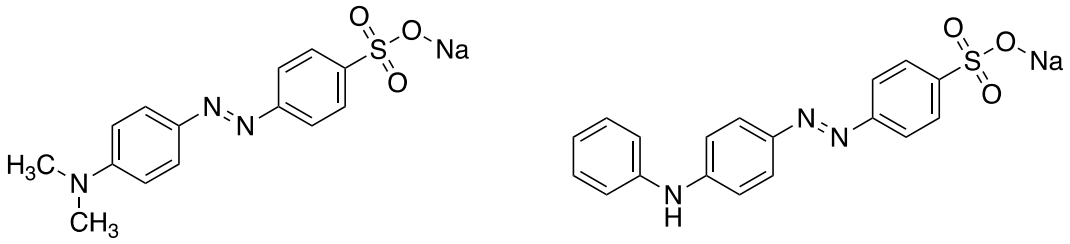


Figure 4. Comparison of dye structures: Methyl Orange (1) and Acid Orange 5 (2).

Methyl Orange (1) and Acid Orange 5 (2) differ in their functional groups, as shown in Figure 4, which affect their interaction mechanisms with HAuNPs. Methyl Orange and Acid Orange 5 are both azobenzene dyes, sharing a common structural core composed of two aromatic rings linked by an azo group (–N=N–). Each dye contains a sulfonate group (SO_3^-)

positioned para to the azo linkage, enhancing water solubility which increases the chance that the dye is absorbed into the particle.[30] Both dye's water-solubility ensures that they can be effectively dissolved in the solution and loaded into the HAuNPs. They can also interact well with the nanoparticle's surface or be encapsulated within the nanoparticle cavity. The dye's primary structural difference lies in the substituents on the opposite benzene ring of the azobenzene core. Methyl Orange features a dimethylamino group, a tertiary amine, while Acid Orange 5 contains a phenylamino group, a secondary amine.

These differences impact both the steric bulk and the protonation behavior of the dyes. The dimethylamino group in Methyl Orange is less bulky and unlikely to become protonated under physiological or mildly acidic conditions, giving it a more hydrophobic and neutral character.[30] In contrast, the secondary amine in Acid Orange 5 can more readily form a conjugate acid in slightly acidic environments, resulting in a positively charged species.[30] This charge can enhance electrostatic interactions with the negatively charged HAuNP surface or cavity.

Additionally, the phenyl ring in Acid Orange 5 introduces greater aromatic surface area, enabling stronger π–π stacking interactions with the nanoparticle surface compared to Methyl Orange.[30] These structural and electronic differences are critical for evaluating how drug-like molecules with varying size, charge, and aromaticity interact with hollow gold nanoparticles. By using these two dyes as models, this study assesses how these molecular features influence loading efficiency and binding strength, as reflected by the equilibrium constant. Molecules with higher loading efficiency and stronger binding (larger equilibrium constants) may exhibit slower release under physiological conditions, as they are more tightly associated with the nanoparticle surface or cavity. In contrast, molecules with lower binding affinity may desorb more readily,

suggesting faster release. Thus, equilibrium binding behavior can serve as a useful predictor of potential release profiles in nanoparticle-based drug delivery systems.

An important aspect of evaluating HAuNPs as drug delivery systems is understanding how drug-like molecules adsorb onto their surfaces. The adsorption of Methyl Orange and Acid Orange 5 onto HAuNPs is modeled using the Langmuir isotherm, which assumes a surface with a fixed number of identical binding sites, each capable of holding one molecule of dye, and no interaction between adsorbed molecules.[31,32] This is essential for determining the loading capacity of the particles for each dye. The key parameters that can be extracted from this model are the equilibrium constant (K), which reflects the affinity between the dye and the nanoparticle surface, and the maximum loading capacity (q_{max}), which indicates the saturation limit. Together, these values will provide insights into the dye-nanoparticle interactions.

The equilibrium reaction is described as a reversible process where the dye molecules interact with the surface, forming a surface-dye complex (Equation c).[33] K can be determined by the ratio of the concentrations of the products (the surface-dye complex) to the concentrations of the reactants (the dye and the surface), as shown in Equation d.[33]

$$Dye + Surface \leftrightarrow Surface \times Dye \quad \text{(c)}$$

$$K = \frac{[Surface \times Dye]}{[Dye][Surface]} \quad \text{(d)}$$

The Langmuir Isotherm equation (Equation e) finds Θ, which is the fractional coverage of the surface, in this case, the fraction of available sites on the HAuNPs that are occupied by the dye.[31] The equilibrium constant describes the affinity between the dye molecules and the nanoparticle surface.[31] This value is important because a larger K value indicates a stronger interaction and more efficient binding of the dye onto the nanoparticles. K can be calculated

from the experimental data and the strength of affinity that Methyl Orange and Acid Orange 5 have on the HAuNP surface can be determined.

$$\Theta = \frac{K[Dye]}{1+K[Dye]} \quad \text{(e)}$$

According to the Langmuir Isotherm, once all the surface sites are occupied, when Θ=1, no more dye can bind to the nanoparticles, leading to a maximum loading capacity (q_{max}).[31] Θ can be calculated by dividing the amount of dye loaded (q) by q_{max} (Equation f).[33]

$$\Theta = \frac{q}{q_{max}} \quad \text{(f)}$$

Combining Equations e and f, the amount of dye loaded (q) is related to the equilibrium dye concentration by Equation g.

$$q = \frac{q_{max}K[Dye]}{1+K[Dye]} \quad \text{(g)}$$

In this experiment, we assume that the equilibrium dye concentration is approximately equal to the initial dye concentration added to the system.[31] This assumption is justified because the amount of dye that binds to the nanoparticles is small compared to the total dye added, due to the relatively low nanoparticle concentration, so the free dye concentration remains effectively unchanged. Therefore, q can be plotted directly against the initial dye concentration to model adsorption behavior and extract parameters such as K and q_{max}.[31]

The process of adsorption is largely determined by non-covalent interactions, including electrostatic forces, van der Waals forces, hydrogen bonding, and hydrophobic interactions.[34] The contribution of each interaction depends on the surface chemistry of the nanoparticles and the chemical properties of the adsorbates. In this study, the use of Tween 20-stabilized HAuNPs introduces surface functional groups, primarily hydrophilic polyoxyethylene chains and

hydrophobic alkyl tails, that influence the strength and nature of dye–nanoparticle interactions.[24] The hydrophilic ethylene oxide groups form a steric and solvation barrier around the nanoparticle surface, which can hinder direct contact between the dye and the gold core, especially for dyes that rely on π–π stacking or electrostatic binding.[24] However, the hydrophobic components of Tween 20 may facilitate weak van der Waals or hydrophobic interactions with dye molecules that have nonpolar or aromatic regions.[24]

These effects can differentially impact Methyl Orange and Acid Orange 5. Methyl Orange, with its dimethylamino group and less bulky structure, has greater hydrophobic character and less steric hindrance, which may allow it to interact more readily with the hydrophobic regions of Tween 20, enhancing its ability to load into the cavity despite the surfactant coating.[24,30] In contrast, Acid Orange 5 has a bulkier phenylamino group and a greater potential for π–π stacking interactions, which may be partially blocked or reduced by the steric effects of the Tween 20 coating.[24,30] As a result, the surface chemistry introduced by Tween 20 may contribute to differences in loading efficiency between the two dyes, by modulating how their structures interact with or are excluded from the nanoparticle surface.

Understanding these adsorption characteristics is essential not only for determining loading efficiency but also for predicting drug release profiles and optimizing nanoparticle design for targeted cancer therapy.

Experimental

Materials

20mM solution of Sodium Borohydride ($NaBH_4$), 10mM solution of Silver Nitrate ($AgNO_3$), 0.1g/L solution of Tween 20, 10.85mM solution of Aqueous Chloroauric Acid ($HAuCl_4$), 200µM solution of Methyl Orange, 200µM solution of Acid Orange 5, pH 7 Phosphate buffer, ultrapure H_2O.

Synthesis of Silver Nanoparticles from Sodium Borohydride

The synthesis of hollow gold nanoparticles (HAuNPs) was adapted from a procedure to make silver nanoparticles (AgNPs). Stock solutions of 10mM Silver Nitrate ($AgNO_3$) and 20mM Sodium Borohydride ($NaBH_4$) were made using ultrapure water. AgNPs were made by measuring out 180mL ultrapure water and combined with 6mL of stock $NaBH_4$ solution to initiate the reaction. The solution was mixed using a magnetic stir bar. While the solution was mixing, 6mL of stock $AgNO_3$ solution was added dropwise. The solution turned a marigold yellow color. The solution was mixed for 20 minutes to ensure that the reaction was complete.

Afterward, the silver nanoparticle solution was centrifuged by adding 15mL of solution to 5mL of 0.1g/L Tween 20 solution in 9 centrifuge tubes. They were centrifuged twice at 6500 rpms for 8 minutes until the supernatant was clear and dark solids were present at the bottom of the tube. The supernatant was removed, and an equivalent volume of Tween solution was added. The tubes were shaken and centrifuged again at 6500 rpms for 8 minutes. The supernatant was removed and replaced by ultrapure water but this time the amount added was half of the volume that was originally in the tube. Silver nanoparticles were confirmed using UV-Vis spectroscopy.

Synthesis of Hollow Gold Nanoparticles from Silver Nanoparticles

30mL of silver nanoparticle solution was measured out into a beaker and began stirring rapidly. While the solution was mixing, 2mL of 10.85mM $HAuCl_4$ solution was added dropwise. The solution turned a clear navy-blue color. HAuNPs were confirmed using UV-Vis Spectroscopy.

Load Dyes to Hollow Gold Nanoparticles

Methyl Orange and Acid Orange 5 were used and combined with HAuNPs. A 200µM stock solution of Methyl Orange and a 200µM stock of Acid Orange 5 were made using pH 7 phosphate buffer. For each dye, seven different dye concentrations were combined with 500µL of HAuNPs in microcentrifuge tubes. The tubes were sonicated and then centrifuged at 6500 rpms for 8 minutes. The supernatants were collected after centrifuging and combined in a graduated cylinder so that the total volume could be recorded from each solution. After removing the supernatant, 1mL of pH 7 phosphate buffer was added to the microcentrifuge tubes containing the nanoparticle pellet, and then they were sonicated and centrifuged again at 6500 rpms for 8 minutes, collecting the new supernatant. This process was repeated for a total of three washes.

Instrumentation

Silver nanoparticles were confirmed within solution by using UV-Vis spectroscopy. The sample was run at room temperature conditions on an Olis-Carey 8453 UV-Vis spectrophotometer. A quartz cuvette was used to perform a scan which was run from 300nm to 600nm to capture the expected peak between 390nm and 430nm of the AgNPs.

Hollow gold nanoparticles were confirmed within solution by using UV-Vis spectroscopy. The sample was run at room temperature conditions on an Olis-Carey 8453 UV-

Vis spectrophotometer. A quartz cuvette was used to perform a scan run from 800nm to 1100nm to capture the expected peak around 980nm of the HAuNPs.

The absorbance of the supernatants of both Methyl Orange and Acid Orange 5 were analyzed using UV-Vis spectroscopy. The samples were run at room temperature conditions on an Olis-Carey 8453 UV-Vis spectrophotometer. A quartz cuvette was used to measure the absorbance at 430nm for Methyl Orange and 434nm for Acid Orange 5.

Results and Discussion

Synthesis of Silver Nanoparticles

The synthesis of AgNPs was successfully carried out using a chemical reduction method with $NaBH_4$ as the reducing agent. Upon the dropwise addition of $AgNO_3$ to the $NaBH_4$ solution under continuous stirring, the reaction mixture turned a distinct marigold yellow color. This color change is attributable to the localized surface plasmon resonance (LSPR) properties of AgNps and is a qualitative indicator of AgNP formation.[35] The reduction reaction of $AgNO_3$ to AgNPs, facilitated by $NaBH_4$, followed Equation a.

$$2AgNO_{3\ (aq)} + 2NaBH_{4\ (aq)} \rightarrow 2Ag^{0}_{(s)} + 2NaNO_{3\ (aq)} + B_2H_{6\ (g)} + H_{2\ (g)} \quad \text{(a)}$$

$NaBH_4$ served as both the reducing agent and a capping agent.[23] During the reduction process, BH_4^- ions were adsorbed onto the surface of the silver nanoparticles, imparting a negative surface charge.[23] This surface charge prevented particle aggregation by electrostatic repulsion, yielding a stable NP solution.[23]

AgNPs have unique optical properties that can be studied through LSPR.[35] This happens when light of specific wavelengths hits the nanoparticles and the electrons on their surface start to vibrate in sync with the light waves.[35] Certain wavelengths of light scatter away from the nanoparticles due to this interaction.[35] This scattering removes certain wavelengths from the light beam, so when the light passes through a UV-Vis spectrometer, those wavelengths are missing and appear as an absorbance peak in the spectrum.[35]

The stability and optical properties of the synthesized AgNPs were characterized using UV-Vis spectroscopy. As shown in Figure 5, a single LSPR resonance peak was observed at approximately 405nm, confirming the formation of AgNPs. This finding is consistent with literature values, where AgNPs synthesized with $NaBH_4$ typically exhibit a resonance peak

between 390nm and 430nm, depending on particle size and shape.[36] These results are also consistent with this study's expectations, as both *Miller* and *Soilis* identified silver nanoparticles with a single resonance peak around 410nm.[37,38] The broadness of the peak indicates that there is some aggregation of the particles and there is a less uniform size distribution.

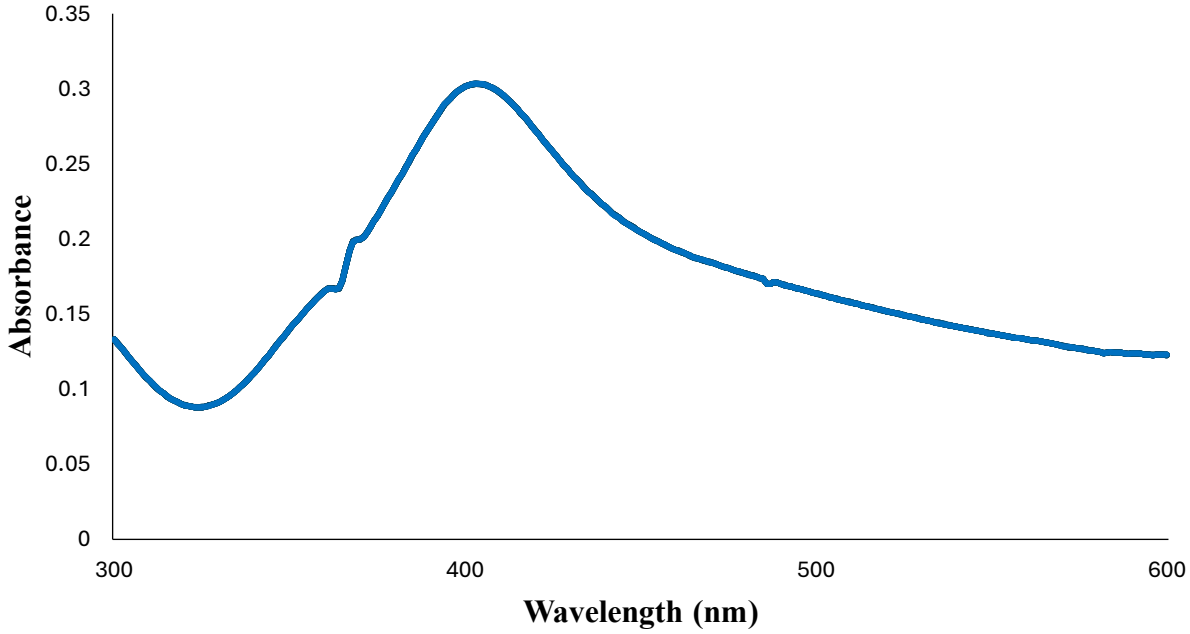


Figure 5. The absorbance spectrum for AgNPs from NaBH4 synthesis after washing. The maximum wavelength is at 405nm, confirming silver nanoparticles.

Synthesis of Hollow Gold Nanoparticles

The synthesized silver nanoparticles were used to make hollow gold nanoparticles. 2mL of 10.85mM $HAuCl_4$ was added dropwise to the solution, resulting in the formation of hollow gold nanoparticles. *Ren et al.* report that when $HAuCl_4$ is added to the silver nanoparticles, a gold shell gradually forms around the AgNPs.[21] Further addition of $HAuCl_4$ fully reduces the silver, creating a hollow gold nanoparticle.[21] HAuNPs can be detected by studying LSPR and each peak will indicate a different nanoparticle structure.[35] Using UV-Vis spectroscopy, *Wang et al.* observed a resonance peak at 957nm.[39] That study used 3-aminopropyltriethoxysilane

(APTES) as a capping agent whereas this study uses Tween 20. *Miller* reported a resonance peak at about 980nm using $NaBH_4$ as a capping agent.[37] A thinner shell or a larger hollow cavity can shift the LSPR peak further into the NIR region.[35] $NaBH_4$'s role as a reducing agent might have created a thinner shell or a larger cavity in the HAuNPs, resulting in a peak further into the NIR region. As shown in Figure 6, a single LSPR resonance peak was observed at 976nm confirming the formation of HAuNPs.

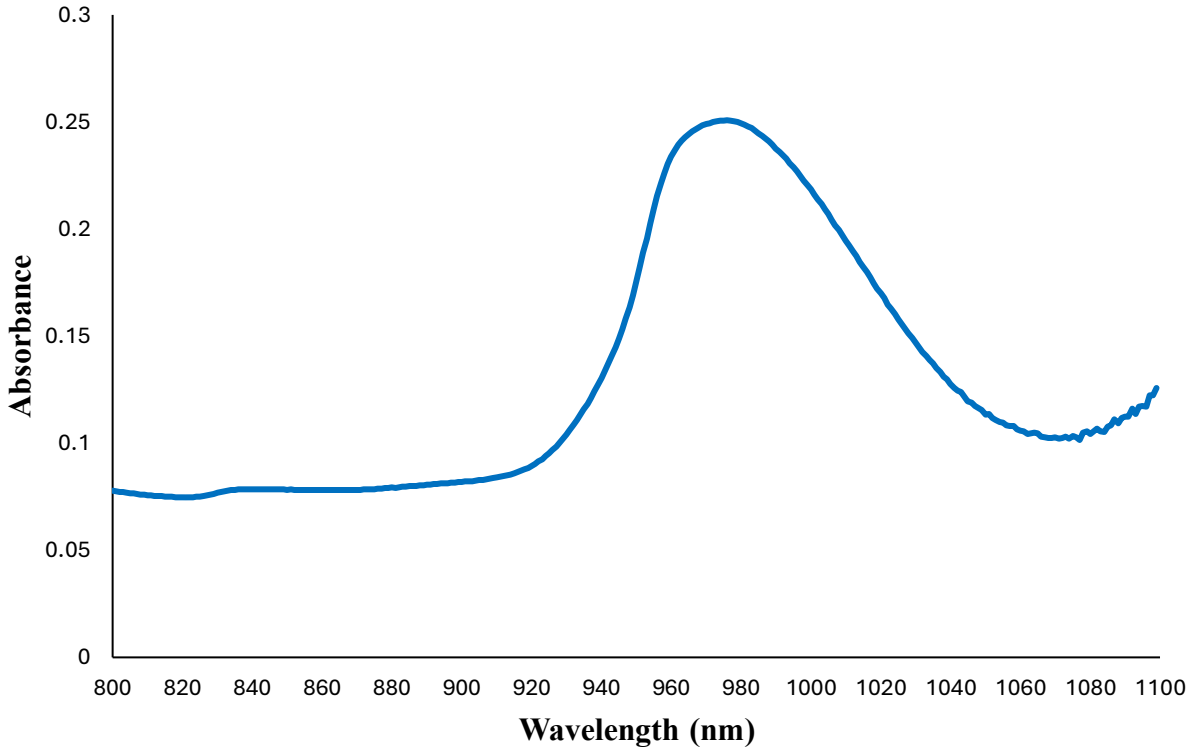


Figure 6. The absorbance spectrum of HAuNPs. The maximum wavelength is at 976nm, confirming hollow gold nanoparticles.

Loading Studies

To understand the loading capacity of HAuNPs, the dyes Methyl Orange and Acid Orange 5 were loaded into HAuNPs to mimic a drug. Using *Miller's* Beer's law calibration curve

for both dyes, the slope of the line of each curve provided the molar absorptivity values (Table 1).[37] Using those values, the concentration of dye in/on the HAuNPs can be found.

Dye	Molar Absorptivity	Maximum Wavelength (nm)
Methyl Orange	0.0122	430
Acid Orange 5	0.0114	434

Table 1. Molar Absorptivity and Maximum Wavelength for dyes Methyl Orange and Acid Orange 5 determined by *Miller*.

To determine the amount of dye loaded onto or into the HAuNPs, the concentration of dye in the supernatant was subtracted from the concentration of dye initially added to the HAuNPs. This calculation follows Equation h.

$$[Dye]_i - [Dye]_f = [Dye]_{in} \quad \text{(h)}$$

The amount of dye loaded into the nanoparticles was converted to nanomoles and was plotted against the concentration of dye initially added and fitted to the Langmuir adsorption isotherm (Equation g). The results for Methyl Orange are shown in Figure 7 and for Acid Orange 5 in Figure 8.

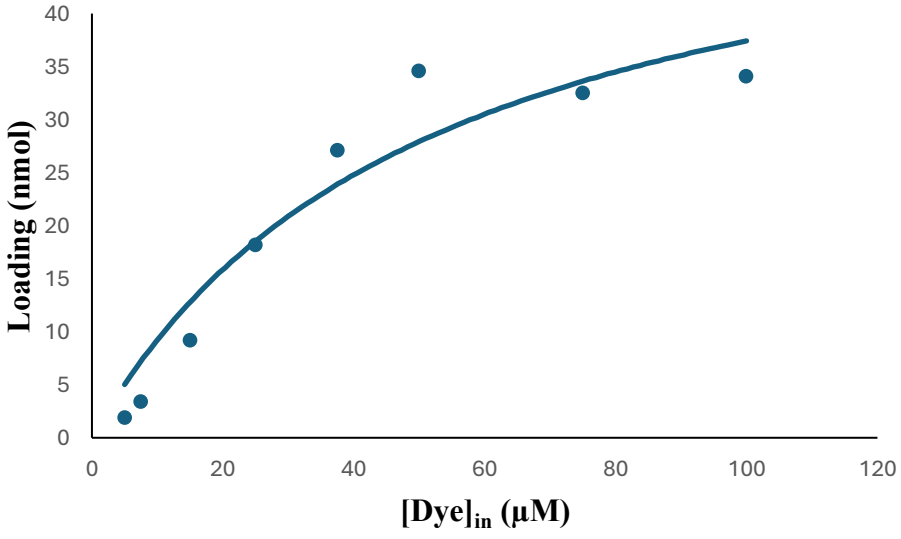


Figure 7. The Langmuir Model for Methyl Orange.

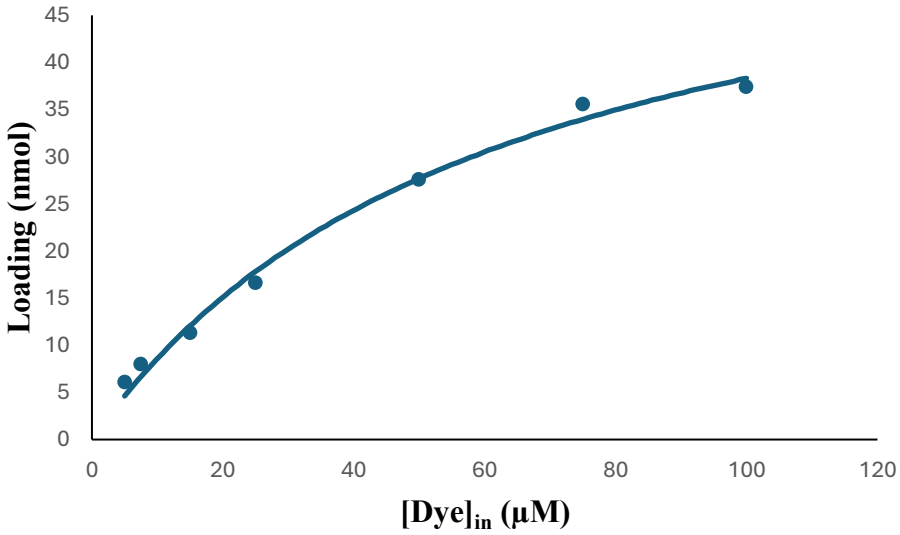


Figure 8. The Langmuir Model for Acid Orange.

The resulting fits yielded the values shown in Table 2.

Dye	q_{max} (µM)	K
Methyl Orange	56.67	0.019
Acid Orange 5	62.19	0.016

Table 2. Langmuir isotherm parameters for Methyl Orange and Acid Orange 5 adsorption onto HAuNPs.

The Langmuir model fit Acid Orange 5 data well, suggesting consistent adsorption behavior across the concentration range. The K value indicated a measurable, but not overly strong, binding affinity, which is a characteristic of reversible interactions like π-π stacking. The secondary aromatic amine and additional phenyl ring increase its potential for π-π stacking interactions with other aromatic groups on the gold nanoparticle surface on the HAuNP surface and with Tween 20.

In contrast, the Methyl Orange data showed a poor fit to the Langmuir model. The isotherm was linear at low concentrations and leveled off quickly, behavior more indicative of a very high K value and a system approaching saturation rapidly. This suggests that Methyl

Orange binds strongly or even irreversibly under the tested conditions, making it difficult to capture the true equilibrium distribution. While the curve could still yield a K value numerically, its interpretation should be approached with caution due to the deviation from ideal Langmuir behavior.

Miller reported Methyl Orange having a K value of 0.022 and Acid Orange 5 having a K value of 0.042. *Miller* also reported that Methyl Orange achieved higher loading concentrations than Acid Orange 5.[37]

The use of Tween 20 as a capping agent in this study introduces a key variable that may influence dye-loading behavior compared to *Miller's* study using uncapped HAuNPs synthesized solely with $NaBH_4$.[37] Tween 20 is a nonionic surfactant composed of a hydrophobic tail and a hydrophilic polyoxyethylene head.[24,25] The polyoxyethylene groups are Lewis bases, which can interact with metal surfaces and stabilize the nanoparticles by steric hindrance and hydration shell formation.[24,25]

This surface capping likely created a more hydrophilic environment around the HAuNPs, potentially altering the adsorption dynamics of the dye molecules.[40] For Methyl Orange, which is smaller and less sterically hindered, this hydrophilic shell may have impeded close contact with the gold surface, reducing binding affinity and leading to a less ideal fit to the Langmuir model. This is supported by the lower K value (0.019) and the deviation from ideal Langmuir behavior, especially the early linear increase and eventual leveling off of dye adsorption. The leveling suggests rapid saturation or competitive interactions that deviate from the assumption of uniform binding sites.

In contrast, Acid Orange 5, with its bulkier and more aromatic structure, may benefit from additional π–π stacking interactions with the nanoparticle surface or Tween 20's aromatic

regions, leading to a better fit with the Langmuir model and a clearer saturation point. The K value for Acid Orange 5 (0.016) is close to that of Methyl Orange, yet the Langmuir fit is stronger, suggesting that the size and shape of the dye molecules become even more important when a capping agent like Tween 20 is present. Methyl Orange, being smaller, may be more affected by the steric barrier created by the Tween 20 layer, while Acid Orange 5, with its bulkier and more aromatic structure, may still interact effectively with the nanoparticle surface despite the capping.

In comparison, *Miller's* uncapped HAuNPs showed higher K values for Acid Orange and better Langmuir model fits overall.[37] This difference underscores how Tween 20 can impact dye-nanoparticle interactions by modifying surface chemistry, altering available binding site accessibility, and introducing steric and solvation effects that are absent in bare nanoparticle systems. While the trends observed in this study highlight the importance of surface chemistry in dye loading behavior, more research is needed to fully understand the interplay between dye structure, nanoparticle capping, and loading efficiency. The findings suggest that Tween 20 alters dye–nanoparticle interactions in complex ways that may not be fully captured by the Langmuir model.

Future Directions

This project can be expanded in several ways. One avenue is to further explore how surface functionalization with capping agents like Tween 20 affects dye–nanoparticle interactions and loading efficiency. Investigating a broader range of capping agents with varying hydrophobicity, chain length, and charge could help clarify how steric hindrance and surface polarity influence adsorption behavior. Additionally, testing a wider range of dye concentrations could better define the true loading capacities of the HAuNPs. This would allow for a more accurate mapping of the full loading curve for both Methyl Orange and Acid Orange 5 and help determine the appropriate adsorption model for Methyl Orange, which did not fit the Langmuir model as well as Acid Orange 5.

Conclusion

This study investigates a potential drug delivery system using hollow gold nanoparticles. The successful synthesis of hollow gold nanoparticles was demonstrated via a galvanic replacement reaction, with the hollow gold nanoparticles exhibiting a localized surface plasmon resonance peak at 976nm. This shows that hollow gold nanoparticles have the potential to be used as drug delivery systems and possible targeted therapy treatment for cancer. Drug molecule loading was simulated through the adsorption of model dyes Methyl Orange and Acid Orange 5. Langmuir Isotherm modeling revealed that Acid Orange 5 showed both a strong fit and high loading capacity, while Methyl Orange deviated from the expected Langmuir behavior, potentially due to rapid surface saturation or non-ideal interactions with the Tween 20-stabilized surface. These differences emphasize the impact of dye structure and surface functionalization on adsorption behavior. Overall, these findings highlight the importance of nanoparticle surface chemistry in tuning loading efficiency and binding strength, which are critical factors in the development of effective, targeted drug delivery systems. Future studies should explore additional capping agents and a broader range of drug analogs to further refine the design of nanoparticle-based therapies.

Resources

(1) John Elflein. *Cancer in the U.S. - Statistics & Facts*. Statista.

(2) Jin, X.; Zhu, Z.; Shi, Y. Metastasis Mechanism and Gene/Protein Expression in Gastric Cancer with Distant Organs Metastasis. *Bull Cancer* **2014**, *101* (1), 1–12. https://doi.org/10.1684/bdc.2013.1882.

(3) Sonkin, D.; Thomas, A.; Teicher, B. A. Cancer Treatments: Past, Present, and Future. *Cancer Genetics*. Elsevier Inc. August 1, 2024, pp 18–24. https://doi.org/10.1016/j.cancergen.2024.06.002.

(4) Ramirez, A.; Towlson, K.; Leaning, M.; Richards, M.; Rubens, R. Do Patients with Advanced Breast Cancer Benefit from Chemotherapy? *Br J Cancer* **1998**, *78* (11), 1488–1494. https://doi.org/10.1038/bjc.1998.711.

(5) Sun, Y.-W.; Wang, L.-H.; Meng, D.-L.; Che, X. A Green and Facile Preparation Approach, Licochalcone A Capped on Hollow Gold Nanoparticles, for Improving the Solubility and Dissolution of Anticancer Natural Product. *Oncotarget* **2017**, *8* (62), 105673–105681. https://doi.org/10.18632/oncotarget.22387.

(6) Abdollahi, S. N.; Naderi, M.; Amoabediny, G. Synthesis and Characterization of Hollow Gold Nanoparticles Using Silica Spheres as Templates. *Colloids Surf A Physicochem Eng Asp* **2013**, *436*, 1069–1075. https://doi.org/10.1016/j.colsurfa.2013.08.028.

(7) Lee, Y. T.; Tan, Y. J.; Oon, C. E. Molecular Targeted Therapy: Treating Cancer with Specificity. *Eur J Pharmacol* **2018**, *834*, 188–196. https://doi.org/10.1016/j.ejphar.2018.07.034.

(8) Siddique, S.; Chow, J. C. L. Gold Nanoparticles for Drug Delivery and Cancer Therapy. *Applied Sciences* **2020**, *10* (11), 3824. https://doi.org/10.3390/app10113824.

(9) Ding, H. M.; Tian, W. De; Ma, Y. Q. Designing Nanoparticle Translocation through Membranes by Computer Simulations. *ACS Nano* **2012**, *6* (2), 1230–1238. https://doi.org/10.1021/nn2038862.

(10) Zhang, S.; Gao, H.; Bao, G. Physical Principles of Nanoparticle Cellular Endocytosis. *ACS Nano*. American Chemical Society September 22, 2015, pp 8655–8671. https://doi.org/10.1021/acsnano.5b03184.

(11) Aftab, S.; Shah, A.; Nadhman, A.; Kurbanoglu, S.; Aysıl Ozkan, S.; Dionysiou, D. D.; Shukla, S. S.; Aminabhavi, T. M. Nanomedicine: An Effective Tool in Cancer Therapy. *International Journal of Pharmaceutics*. Elsevier B.V. April 5, 2018, pp 132–149. https://doi.org/10.1016/j.ijpharm.2018.02.007.

(12) Damani, M.; Desai, N.; Singh, B. P.; Ningthoujam, R. S.; Momin, M.; Khan, T. Synthesis of Hollow Gold Nanoparticles - Impact of Variables on Process Optimization. *J Pharm Sci* **2022**, *111* (10), 2907–2916. https://doi.org/10.1016/j.xphs.2022.08.003.

(13) Yasun, E.; Gandhi, S.; Choudhury, S.; Mohammadinejad, R.; Benyettou, F.; Gozubenli, N.; Arami, H. Hollow Micro and Nanostructures for Therapeutic and Imaging Applications. *Journal of Drug Delivery Science and Technology*. Editions de Sante December 1, 2020. https://doi.org/10.1016/j.jddst.2020.102094.

(14) Karimi, M.; Sahandi Zangabad, P.; Baghaee-Ravari, S.; Ghazadeh, M.; Mirshekari, H.; Hamblin, M. R. Smart Nanostructures for Cargo Delivery: Uncaging and Activating by Light. *Journal of the American Chemical Society*. American Chemical Society April 5, 2017, pp 4584–4610. https://doi.org/10.1021/jacs.6b08313.

(15) Dung, N. T.; Linh, N. T. N.; Chi, D. L.; Hoa, N. T. H.; Hung, N. P.; Ha, N. T.; Nam, P. H.; Phuc, N. X.; Tam, L. T.; Lu, L. T. Optical Properties and Stability of Small Hollow Gold Nanoparticles. *RSC Adv* **2021**, *11* (22), 13458–13465. https://doi.org/10.1039/d0ra09417j.

(16) You, J.; Zhang, G.; Li, C. Exceptionally High Payload of Doxorubicin in Hollow Gold Nanospheres for Near-Infrared Light-Triggered Drug Release. In *ACS Nano*; 2010; Vol. 4, pp 1033–1041. https://doi.org/10.1021/nn901181c.

(17) Sheth, R. A.; Wen, X.; Li, J.; Melancon, M. P.; Ji, X.; Andrew Wang, Y.; Hsiao, C. H.; Chow, D. S. L.; Whitley, E. M.; Li, C.; Gupta, S. Doxorubicin-Loaded Hollow Gold Nanospheres for Dual Photothermal Ablation and Chemoembolization Therapy. *Cancer Nanotechnol* **2020**, *11* (1). https://doi.org/10.1186/s12645-020-00062-8.

(18) Mastria, E. M.; Cai, L. Y.; Kan, M. J.; Li, X.; Schaal, J. L.; Fiering, S.; Gunn, M. D.; Dewhirst, M. W.; Nair, S. K.; Chilkoti, A. Nanoparticle Formulation Improves Doxorubicin Efficacy by Enhancing Host Antitumor Immunity. *Journal of Controlled Release* **2018**, *269*, 364–373. https://doi.org/10.1016/j.jconrel.2017.11.021.

(19) You, J.; Shao, R.; Wei, X.; Gupta, S.; Li, C. Near-Infrared Light Triggers Release of Paclitaxel from Biodegradable Microspheres: Photothermal Effect and Enhanced Antitumor Activity. *Small* **2010**, *6* (9), 1022–1031. https://doi.org/10.1002/smll.201000028.

(20) Xiong, C.; Lu, W.; Zhou, M.; Wen, X.; Li, C. Cisplatin-Loaded Hollow Gold Nanoparticles for Laser-Triggered Release. *Cancer Nanotechnol* **2018**, *9* (1). https://doi.org/10.1186/s12645-018-0041-9.

(21) Ren, Q.-Q.; Bai, L.-Y.; Zhang, X.-S.; Ma, Z.-Y.; Liu, B.; Zhao, Y.-D.; Cao, Y.-C. Preparation, Modification, and Application of Hollow Gold Nanospheres. *J Nanomater* **2015**, *2015* (1). https://doi.org/10.1155/2015/534070.

(22) Park, J. M.; Choi, H. E.; Kudaibergen, D.; Kim, J. H.; Kim, K. S. Recent Advances in Hollow Gold Nanostructures for Biomedical Applications. *Frontiers in Chemistry*. Frontiers Media S.A. June 8, 2021. https://doi.org/10.3389/fchem.2021.699284.

(23) Biegel, M.; Schikarski, T.; Cardenas Lopez, P.; Gromotka, L.; Lübbert, C.; Völkl, A.; Damm, C.; Walter, J.; Peukert, W. Efficient Quenching Sheds Light on Early Stages of Gold Nanoparticle Formation. *RSC Adv* **2023**, *13* (26), 18001–18013. https://doi.org/10.1039/d3ra02195e.

(24) Chang, C. W.; Tseng, W. L. Gold Nanoparticle Extraction Followed by Capillary Electrophoresis to Determine the Total, Free, and Protein-Bound Aminothiols in Plasma. *Anal Chem* **2010**, *82* (7), 2696–2702. https://doi.org/10.1021/ac902342c.

(25) Zhou, H.; Zheng, L.; Jia, H. Facile Control of the Self-Assembly of Gold Nanoparticles by Changing the Capping Agent Structures. *Colloids Surf A Physicochem Eng Asp* **2014**, *450* (1), 9–14. https://doi.org/10.1016/j.colsurfa.2014.03.013.

(26) Lu, F.; Xin, H.; Xia, W.; Liu, M.; Zhang, Y.; Cai, W.; Gang, O. Tailoring Surface Opening of Hollow Nanocubes and Their Application as Nanocargo Carriers. *ACS Cent Sci* **2018**, *4* (12), 1742–1750. https://doi.org/10.1021/acscentsci.8b00778.
(27) Fathordoobady, F.; Sannikova, N.; Guo, Y.; Singh, A.; Kitts, D. D.; Pratap-Singh, A. Comparing Microfluidics and Ultrasonication as Formulation Methods for Developing Hempseed Oil Nanoemulsions for Oral Delivery Applications. *Sci Rep* **2021**, *11* (1), 72. https://doi.org/10.1038/s41598-020-79161-w.
(28) Tropaeolin OO _ C18H14N3NaO3S _ CID 23668839 - PubChem.
(29) Methyl Orange _ C14H14N3NaO3S _ CID 23673835 - PubChem.
(30) Georgeous, J.; AlSawaftah, N.; Abuwatfa, W. H.; Husseini, G. A. Review of Gold Nanoparticles: Synthesis, Properties, Shapes, Cellular Uptake, Targeting, Release Mechanisms and Applications in Drug Delivery and Therapy. *Pharmaceutics*. Multidisciplinary Digital Publishing Institute (MDPI) October 1, 2024. https://doi.org/10.3390/pharmaceutics16101332.
(31) Azizian, S.; Eris, S.; Wilson, L. D. Re-Evaluation of the Century-Old Langmuir Isotherm for Modeling Adsorption Phenomena in Solution. *Chem Phys* **2018**, *513*, 99–104. https://doi.org/10.1016/j.chemphys.2018.06.022.
(32) Latour, R. A. The Langmuir Isotherm: A Commonly Applied but Misleading Approach for the Analysis of Protein Adsorption Behavior. *J Biomed Mater Res A* **2015**, *103* (3), 949–958. https://doi.org/10.1002/jbm.a.35235.
(33) *Derivation of the Langmuir Isotherm*.
(34) Zhou, R.; Wang, Y.; Zhang, D.; Ye, P.; Wei, J. Study on the Adsorption Mechanism of Hydrophobic SiO_2 Nanoparticles: A Molecular Dynamics Study. *Energy Sci Eng* **2025**, *13* (1), 355–364. https://doi.org/10.1002/ese3.2004.
(35) Hamamoto, M.; Yagyu, H. Particle Size Distribution and Au Concentration Dependence of the Refractive-Index Sensitivity of LSPR Sensors Based on Gold Nanoparticles. *Journal of Nanoparticle Research* **2023**, *25* (8). https://doi.org/10.1007/s11051-023-05802-6.
(36) Khatoon, U. T.; Velidandi, A.; Nageswara Rao, G. V. S. Sodium Borohydride Mediated Synthesis of Nano-Sized Silver Particles: Their Characterization, Anti-Microbial and Cytotoxicity Studies. *Mater Chem Phys* **2023**, *294*. https://doi.org/10.1016/j.matchemphys.2022.126997.
(37) Miller, H. *Investigation of a Potential Drug Delivery System Using Hollow Gold Nanoparticles Hana Miller Senior Comprehensive Project Investigation of a Potential Drug Delivery System Using Hollow Gold Nanoparticles*; 2023.
(38) Soilis, Z. M. *Alizarin Red S Loaded Poly (Vinyl Pyrrolidone) Capped Hollow Gold Nanoparticles: A Model Drug Delivery Device*; 2020.
(39) Wang, Y. C.; Rhéaume, É.; Lesage, F.; Kakkar, A. Synthetic Methodologies to Gold Nanoshells: An Overview. *Molecules*. MDPI AG November 2, 2018. https://doi.org/10.3390/molecules23112851.
(40) Rudel, H. E.; Zimmerman, J. B. Elucidating the Role of Capping Agents in Facet-Dependent Adsorption Performance of Hematite Nanostructures. *ACS Appl Mater Interfaces* **2023**, *15* (29), 34829–34837. https://doi.org/10.1021/acsami.3c05104.